Highly Crystalline Activated Layered Double Hydroxides as Solid Acid-Base Catalysts

Xiaodong Lei, Fazhi Zhang, Lan Yang, Xiaoxiao Guo, Yuanyuan Tian, Shanshan Fu, Feng Li, David G. Evans, and Xue Duan
State Key Laboratory of Chemical Resource Engineering, Beijing University of Chemical Technology, Beijing 100029, China

DOI 10.1002/aic.11118
Published online February 16, 2007 in Wiley InterScience (www.interscience.wiley.com).

Activated layered double hydroxides (LDHs) with high crystallinity, obtained by calcination/rehydration of LDH precursors synthesized by urea decomposition, have higher catalytic activity in acetone self-condensation and Knoevenagel reactions than less crystalline materials obtained from LDH precursors synthesized by titration co-precipitation. The activated LDHs possess both basic and acidic sites. High resolution transmission electron microscopy (HRTEM) confirms that the highly crystalline activated LDHs retain the lattice structure of the LDH precursors with lattice parameters $a = b = 0.31 \pm 0.01$ *nm and* $\alpha = 60 \pm 2^{\circ}$. *An acid-base catalytic mechanism has been proposed to interpret the catalytic behavior based on the fact that acid-base hydroxyl group pairs on the activated LDH surface have a separation of 0.31 nm. It is proposed that the active sites are mainly located on the ordered array of hydroxyl sites on the basal surfaces rather than on the edges, as has been previously suggested.*
 AIChE J, 53: 932–940, 2007
Keywords: layered double hydroxides, hydrotalcite, urea decomposition, aldol reaction, Knoevenagel reaction

Introduction

Although a great many very efficacious heterogeneous catalysts have been prepared,[1] identification of the actual active sites in any given catalyst presents a considerable challenge.[2] Advances in high-resolution microscopy[3] and in situ spectroscopy,[4] along with theoretical studies,[5] have led to considerable progress in our understanding, although many issues remain unresolved.[6] Catalytic activity is often ascribed to the presence of defect surface sites with unusually low coordination number, or ensembles of contiguous surface sites.[5,7] For example, in the case of a layered material such as MoS_2 which has platelet-like crystals, cleavage parallel to the basal planes produces a highly inert surface with coordinatively saturated Mo atoms, whilst cleavage perpendicular to the basal planes generates edge surfaces with coordinatively unsaturated Mo sites which have high activity as hydrodesulfurization catalysts.[7,8] In the case of catalysis by solid acids and bases, Iglesia et al.[9] have postulated that bifunctional pathways, which require that different sites co-exist within molecular distances, are often involved and Climent et al.[10] have proposed a bifunctional acid-base mechanism for the condensation of heptanal with benzaldehyde over amorphous aluminophosphate. Here, we describe the catalytic activity of layered double hydroxide (LDH) materials in acetone self-condensation and the Knoevenagel reaction and propose that the active sites are located on the ordered array of hydroxyl sites on the basal surfaces rather than on defect sites associated with the edges, as has been previously suggested.

Layered double hydroxides (LDHs), also known as hydrotalcite-like materials or synthetic anionic clays, have a brucite-like structure and the formula $[M^{II}_{1-x}M^{III}_{x}(OH)_2]^{x+}$

Correspondence concerning this article should be addressed to X. Duan at duanx@mail.buct.edu.cn.

$(A^{n-})_{x/n} \cdot yH_2O$. Isomorphous replacement of some of the M^{II} cations by M^{III} produces layers with a positive charge which is compensated by anions located, along with water molecules, in the interlayer galleries.[11] LDHs have attracted increasing attention in recent years owing to their potential applications as adsorbents, ionic conductors, and catalysts.[11] On thermal decomposition of LDHs at about 750 K, a mixed oxide phase is obtained which has high base catalytic activity. This material may be rehydrated, resulting in regeneration of the layered structure with the original interlayer anions being replaced by OH^- ions. The resulting so-called activated LDHs are known to be effective solid catalysts for the Claisen-Schmidt[12] and Knoevenagel[13] condensations, and the Wittig[14] and Henry[15] reactions. The aldol codensation of acetone to afford diacetone alcohol (DAA) has been widely used[16–23] to study the catalytic activity of activated LDHs, but conclusive relationships between the preparation procedure, surface area, number, and nature of active OH groups and activity have not been derived.[22] Very recently, Kaneda and coworkers.[24] have suggested that activated LDHs provide a unique acid-base bifunctional surface capable of promoting the Knoevenagel and Michael reactions of nitriles with carbonyl compounds. In the studies reported to date,[16–23] the LDH precursors were obtained by traditional co-precipitation methods. Poorly crystalline samples with particle sizes below 0.5 μm are generally obtained by this procedure, unless the materials are aged under hydrothermal conditions. LDHs with higher crystallinity can be prepared, however, by precipitation from homogeneous solution using the temperature-controlled hydrolysis of urea, which gives the required gradual increase in both pH and concentration of carbonate ions.[25–28]

In this article, the structural, textural, and basic properties of samples of MgAl-OH LDH materials obtained by calcination/rehydration of MgAl-CO_3 LDH precursors with high crystallinity are described. For comparison, MgAl-CO_3-LDHs were also prepared by the traditional titration co-precipitation method and the corresponding activated samples obtained by the same calcination/rehydration procedure. The catalytic properties of the two rehydrated samples were evaluated using the self-condensation of acetone at 273 and 293 K and the Knoevenagel reaction of malononitrile with benzaldehyde. A base-acid catalytic mechanism is proposed to interpret the catalytic behavior.

Experimental

Catalyst preparation

The urea decomposition method was used to prepare MgAl-CO_3 LDHs with Mg^{2+}/Al^{3+} molar ratio of 2. $Mg(NO_3)_2 \cdot 6H_2O$ and $Al(NO_3)_3 \cdot 9H_2O$ were dissolved in deionized water (75 mL) to give solutions with a total concentration of metal cations of 0.3 M which were placed in polytetrafluoroethylene vessels. Urea ([urea]/[NO_3^-] = 4) was dissolved in the above solution. The containers were sealed and placed in an oven and maintained at 363 K for either 3 or 10 d. The solutions were allowed to cool, the solid was collected by filtration and washed with deionized water and subsequently dried at 373 K for 24 h (denoted as U-LDH(3) and U-LDH(10), respectively). The resulting MgAl-CO_3-LDHs were heated in an N_2 flow to 773 K with a heating rate of 10 K/min and kept at that temperature for 8 h. The resulting solids (denoted U-LDO(3) and U-LDO(10), respectively) were then dispersed in decarbonated water for 5 h under N_2. Excess water was removed by decantation and the sample dried under vacuum. The activated MgAl-OH-LDHs prepared by this method are denoted as U-RLDH(3) and U-RLDH(10), respectively.

For comparison purposes, an MgAl-CO_3 LDH with Mg^{2+}/Al^{3+} molar ratio of 2 was synthesized by a conventional titration co-precipitation method. $Mg(NO_3)_2 \cdot 6H_2O$ and $Al(NO_3)_3 \cdot 9H_2O$ were dissolved in deionized water (100 mL) to give a solution with a total concentration of metal cations of 0.6 M. The metal salt solution was titrated into 100 mL of a solution containing 1.2 M NaOH and 0.1 M Na_2CO_3 at 313 K with vigorous stirring. When the addition was complete, the mixture was aged at 363 K for 24 h. The resulting MgAl-CO_3-LDH is designated as T-LDH. Calcination and rehydration were carried out using the same procedures as that for the sample synthesized by urea decomposition method to give materials denoted as T-LDO and T-RLDH, respectively.

Characterization

Powder X-ray diffraction (XRD) patterns were obtained in the 2θ range 3–70° using a Shimadzu XRD-6000 instrument with Cu Kα source (λ = 0.15406 nm). Scanning electron micrographs (SEM) were recorded on a Hitachi S-3500N SEM instrument. All SEM samples were sputtered with gold. Transmission electron microscopy (TEM) images and high resolution transmission electron microscopy (HRTEM) images were obtained using a JEOL JEM-2100 transmission electron microscope. The particle size distribution was determined using a Malvern Mastersizer 2000 laser particle size analyzer. Doubly deionized water was used as dispersion medium and the mixture treated ultrasonically. Elemental analyses for Mg and Al were performed with a Shimadzu ICPS-7500 inductively coupled plasma spectroscopy (ICP) instrument on solutions prepared by dissolving the samples in dilute HNO_3 (1:1). The carbon content was determined using a Vario EL III elemental analyzer (EA). The low-temperature N_2 adsorption-desorption experiments were carried out using a Quantachrome Autosorb-1 system. Samples were outgassed at 353 K for 8 h. The pore size distributions were calculated from desorption isotherms by the Barrett-Joyner-Hallender (BJH) method, and the specific surface areas were calculated using the Brunauer-Emmett-Teller (BET) method based on the N_2 adsorption isotherms. Simultaneous thermogravimetric and differential thermal analysis (TG-DTA) were carried out in air on a PCT-1A thermal analysis system produced locally. Samples of 9.0–10.0 mg were heated at 10 K/min up to 873 K.

Determination of acidic and basic properties

The adsorption isotherms at 298 K of phenol dissolved in cyclohexane were used to estimate the surface base properties of the RLDH catalysts. The amount of phenol adsorbed by the catalysts was measured by UV spectroscopy (λ_{max} = 271.6 nm) on a Shimadzu UV-2501PC UV-Visible recording

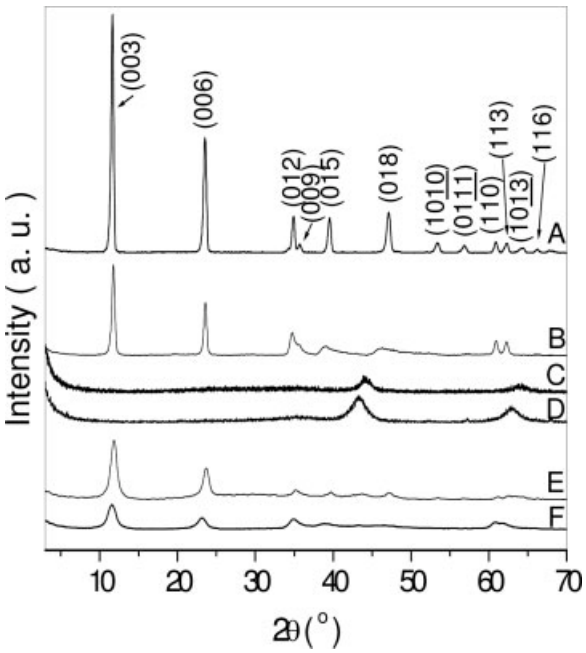

Figure 1. XRD patterns of different samples: (A) U-LDH (3), (B) T-LDH, (C) U-LDO(3), (D) T-LDO, (E) U-RLDH(3), and (F) T-RLDH.

spectrophotometer. The ratio of cyclohexane solution/catalyst was 50 mL/0.1 g.

The surface acidity of RLDHs was investigated by adsorption of pyridine on self-supporting wafers (10 mg/cm^2). Fourier transform infrared (FTIR) spectra of adsorbed samples were recorded in the range 1700–1400 cm^{-1} with 2 cm^{-1} resolution on a Bruker Vector-22 spectrometer. The self-supporting wafer was placed between two CaF_2 windows. The wafers were degassed at 373 K for 2 h at 10^{-4} N/m^2, prior to the adsorption of pyridine. The pyridine was adsorbed on the surface of the samples at room temperature for 30 min, which were then outgassed at 373 K for 2 h at 10^{-4} N/m^2. The FTIR measurements were performed at room temperature.

Catalytic testing

The self-condensation of acetone was performed at 273 K (maintained by use of an ice bath) and at room temperature (293 K) under an N_2 atmosphere in lightly agitated 250 mL three-necked flasks. A given amount of acetone and 0.3 g of freshly activated catalyst were added under a flow of N_2 to exclude atmospheric carbon dioxide (CO_2). The mixture of products was analyzed by a gas chromatograph-mass spectrometer (GCMS-QP2010, Shimadzu). Iso-octane was used as an internal standard to calculate the amount of DAA formed.

The Knoevenagel reaction of malononitrile with benzaldehyde was performed at 333 K. To the reaction vessel containing the RLDHs (0.3 g) was added DMF (4 mL), malononitrile (20 mmol), and benzaldehyde (20 mmol). After the reaction mixture was stirred for a given time, the RLDHs was separated by filtration. The mixture of products was analyzed by GCMS using n-decane as internal standard to calculate the yield of benzylidenemalononitrile.

Results and Discussion

Structure of catalysts and their precursors

The XRD patterns of the samples obtained by urea decomposition (U-LDH) and titration co-precipitation (T-LDH) are shown in Figures 1A, B, respectively, and are consistent with those reported in the literature.[25,27] The greater intensities and narrower line-widths of the peaks for U-LDH indicate that, as previously reported,[27] the material is much more crystalline than T-LDH. After calcination at 773 K, the two LDO samples exhibit the characteristic peaks of poorly crystalline MgO structure (Figures 1C, D) in accordance with reports in the literature.[16–18] When the calcined samples are rehydrated in decarbonated water, the XRD patterns (Figures 1E, F) of the resulting RLDHs reveal that the LDH structure has been regenerated. Rehydration of the calcined samples resulting in the reconstruction of the layered structure is often described as a "memory effect."[16–18] In the powder XRD patterns, the basal reflections (003) and (006) of the U-RLDH(3) are stronger and sharper than those of T-RLDH (See Table 1), indicating that the crystallinity of the latter is lower.

SEM and TEM images (shown in Figure 2) were recorded to investigate the morphology of the samples. The micrograph of U-LDH(3) prepared by the urea method (Figure 2A) shows well-developed hexagonal plates with fairly large particle sizes (2–4 μm). Such a finding can be rationalized by considering the slow rate of hydrolysis of urea.[27,28] The morphology and particle size of the calcined material LDO(3) (Figure 2B) and the corresponding rehydrated U-RLDH(3) (Figure 2C) are similar to those of the U-LDH(3) precursor. Figure 2D shows the TEM image of T-RLDH from which it is clear that, compared with U-RLDH, T-RLDH has much smaller particle size and irregular platelet morphology.

Figures 3A, B show the HRTEM images of the LDH precursor U-LDH (3) synthesized using the urea method. The periodicity of bright spots confirms the presence of a two-dimensional lattice with $a = b = 0.31 \pm 0.01$ nm and $\alpha = 60 \pm 2°$. The bright spots correspond to the hydroxyl groups or external oxygen atoms of the LDH. Yao et al. have obtained similar results by AFM and STM.[29,30] Figures 3C, D that show the HRTEM images of U-RLDH(3) have the same periodicity of bright spots as the as-synthesized LDH precursor. This indicates that U-RLDH retains the lattice structure of the LDH precursor. These data confirm that the

Table 1. Peakwidths (Full Width at Half-Maximum, FWHM) for Different Diffraction Peaks of U-RLDH(3) and T-RLDH

	FWHM for (003)	FWHM for (006)	FWHM for (012)	FWHM for (015)	FWHM for (018)
U-RLDH(3)	0.781	0.822	0.800	1.010	1.312
T-RLDH	0.953	0.975	1.113	1.767	2.300

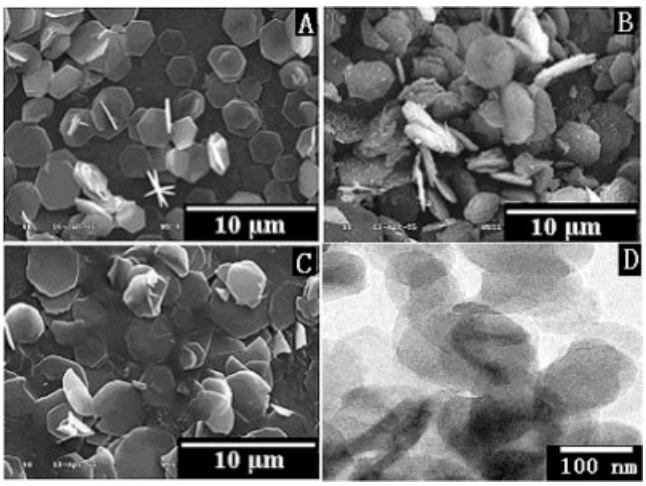

Figure 2. SEM images of U-LDH(3) (A), U-LDO(3) (B), U-RLDH (3) (C), and TEM image of T-RLDH (D).

distances between adjacent hydroxyl pairs are 0.31 nm. The lattice structure of T-RLDH cannot be seen clearly using the same HRTEM instrument because of its poor crystallinity (See Figure 4).

The particle size distribution curves for the two rehydrated samples U-RLDH(3) and T-RLDH are illustrated in Figure 5. The average particle sizes of U-RLDH(3) and T-RLDH are 3.5 and 0.25 μm, respectively, which is in agreement with the results of SEM and TEM.

The low temperature N_2 adsorption-desorption isotherms and BJH desorption pore diameter distributions of the two rehydrated samples U-RLDH(3) and T-RLDH are shown in Figure 6. The isotherms of both samples (Figures 6A, C) show similar features characteristic of type IV with a broad

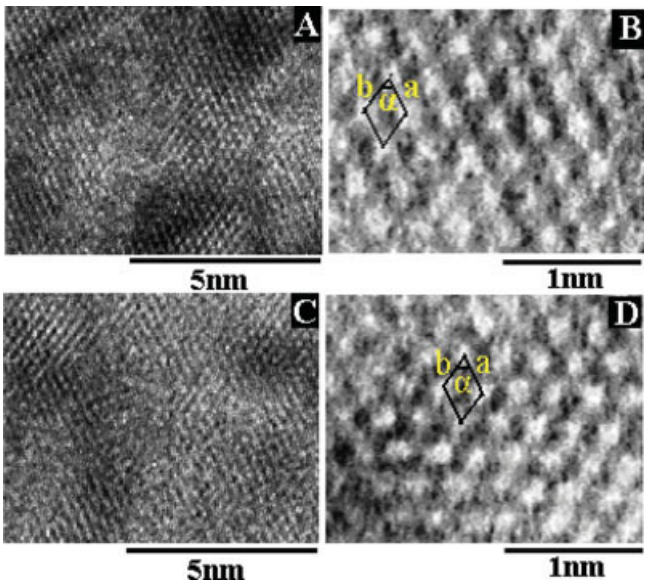

Figure 3. HRTEM images of U-LDH(3) (A, B) and corresponding U-RLDH (3) (C, D).

[Color figure can be viewed in the online issue, which is available at www.interscience.wiley.com.]

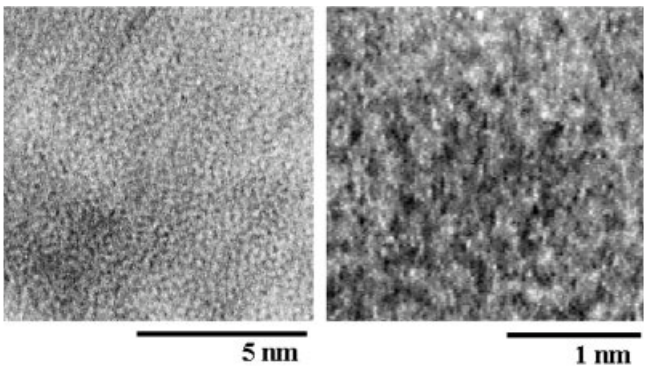

Figure 4. HRTEM images of T-RLDH.

H_3 type hysteresis loop according to the BDDT (Brunauer, Deming, Deming, and Teller) classification,[31] which is generally observed for plate-like particles with slit-shaped pores. Figures 6B, D show that the pore diameter distributions of U-RLDH(3) and T-RLDH are both relatively narrow. The BET surface area of U-RLDH(3) (~141 $m^2\ g^{-1}$) is lower than T-RLDH (~185 $m^2\ g^{-1}$), consistent with the higher crystallinity and larger particle size of the former material.

The TG-DTA data for U-RLDH(3) and T-RLDH are illustrated in Figure 7. U-RLDH(3) undergoes a weight loss of 15.8% from 303 to 513 K (Figure 7A) accompanied by an endothermic peak in the DTA observed at 510 K (Figure 7C). A second weight loss of 25.1% occurs between 513 K and 773 K with a weak endothermic peak at 690 K. For T-RLDH (Figure 7B), two weight loss peaks are also observed. The first one from 303 to 513 K corresponds to a 14.9% weight loss and the second one, from 513 to 773 K, to 25.7%. The first endothermic peak in the DTA (Figure 7D) is found at 504 K and the second endothermic is very weak at about 674 K. A two-step weight loss is generally observed for LDHs.[32] The first one is ascribed to removal of water physisorbed on the external surface of the crystallites as well as water intercalated in the interlayer galleries and the second weight loss to dehydroxylation of the layers and loss of

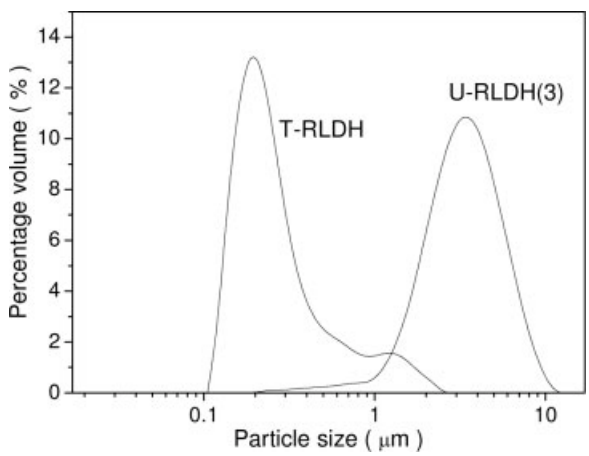

Figure 5. Particle sizes of RLDH samples.

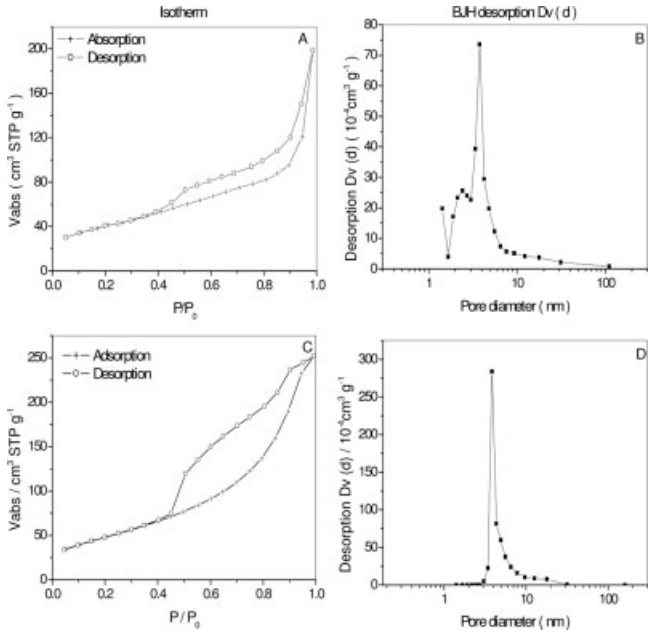

Figure 6. N_2 adsorption-desorption isotherms and pore diameter distributions of U-RLDH (3) (A, B) and T-RLDH (C, D).

volatile species arising from decomposition of interlayer anions.

Basic and acid properties

The acid-base properties of catalysts derived from LDHs have been studied by a number of workers.[33] The results of

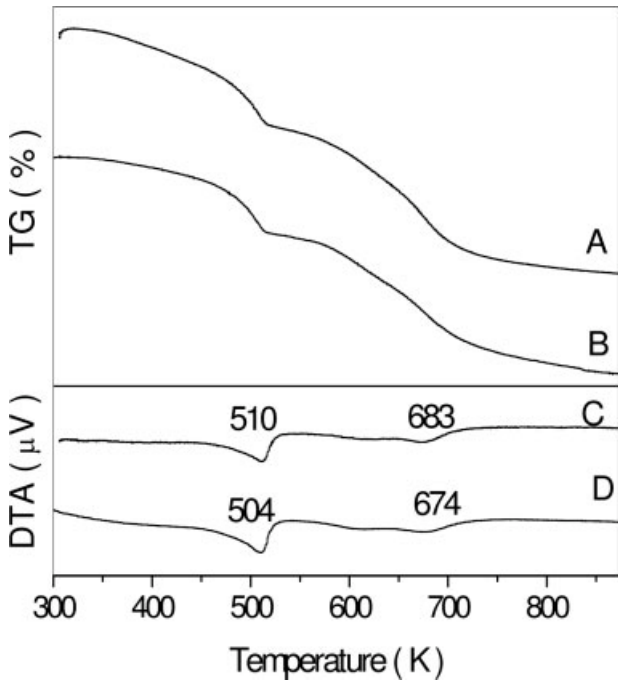

Figure 7. TG-DTA curves for U-RLDH (3) (A, C) and T-RLDH (B, D).

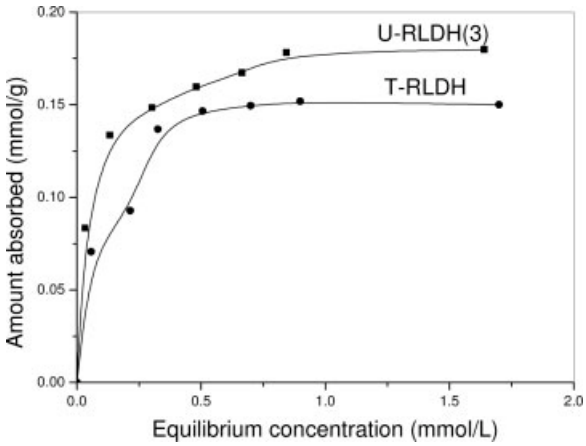

Figure 8. Adsorption isotherms for phenol from cyclohexane solution on catalysts.

CO_2 and NH_3 TPD experiments and FTIR spectroscopy, using CO_2 and NH_3 as probe molecules have been reported,[34,35] and the surface basicity and acidity of as-prepared and calcined LDHs has also previously been investigated by means of adsorption isotherms of phenol from cyclohexane solution,[36,37] and adsorption of pyridine monitored using IR spectroscopy,[38,39] respectively. The basic properties of U-RLDHs and T-RLDH were investigated by studying the adsorption isotherms for phenol from cyclohexane solution at 298 K following the procedure reported in the literature.[36,37] The adsorption isotherms are shown in Figure 8. LDHs are characterized by a Brønsted basicity associated with the OH^- anions and by a very weak Lewis acidity because of their hydration.[33] Figure 8 indicates that, although the surface area of U-RLDH(3) is lower than that of T-RLDH, the overall number of basic sites on the U-RLDH(3) exceeds that in T-RLDH. This presumably reflects the ordered array and consequent high density of basic hydroxyl sites on the basal surfaces of U-RLDH(3) shown by HRTEM (Figure 3). We also studied the surface acidity of RLDHs by

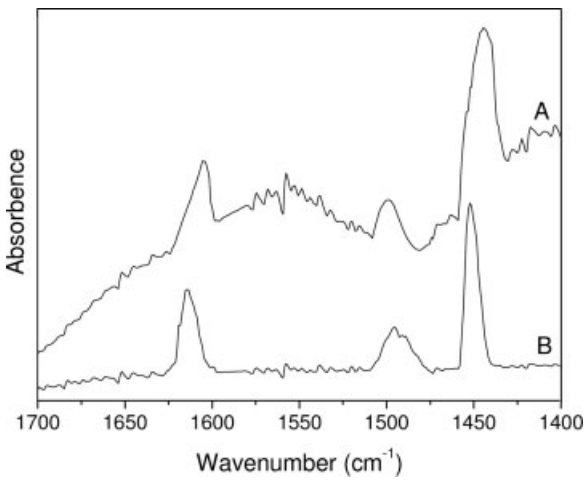

Figure 9. FTIR spectra recorded after adsorption of pyridine on U-RLDH (3) (A) and T-RLDH (B).

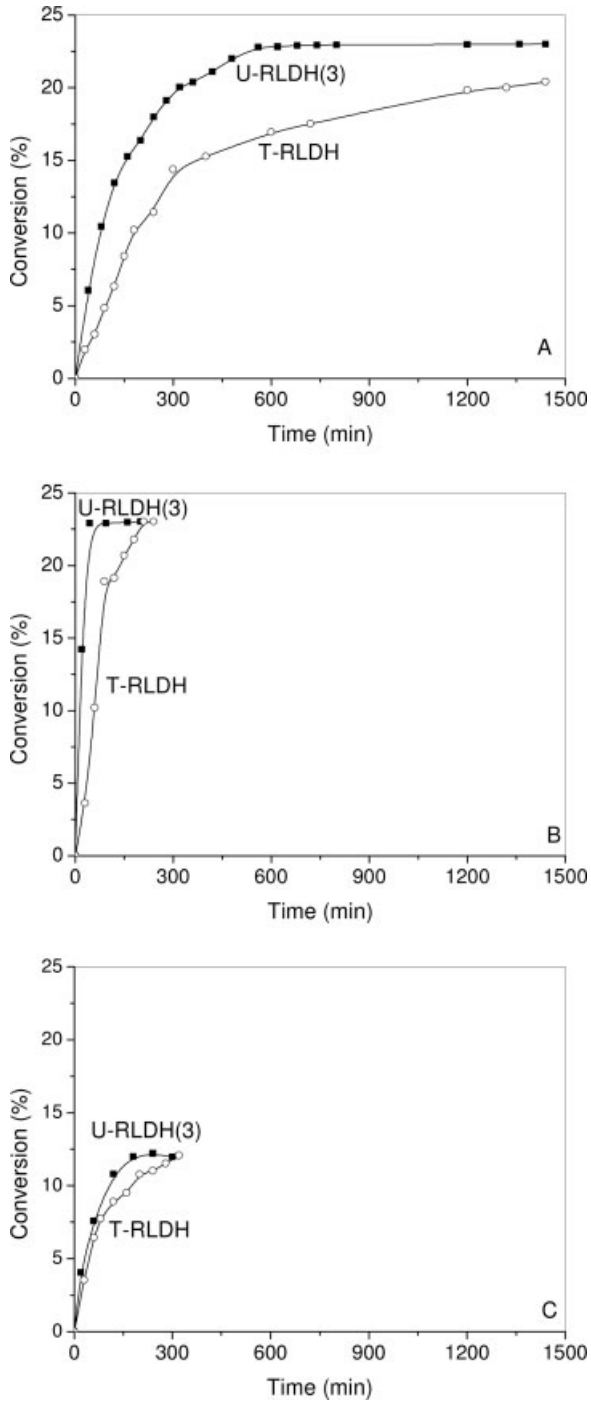

Figure 10. Conversion of acetone to DAA with different catalysts: (A) reaction at 273 K with acetone/catalyst = 2 mol/0.3 g; (B) reaction at 273 K with acetone/catalyst = 0.075 mol/0.3 g; (C) reaction at 293 K with acetone/catalyst = 2 mol/0.3 g.

the adsorption of pyridine monitored using IR spectroscopy. Samples were degassed at 373 K for 2 h at 10^{-4} N/m^2, prior to the adsorption of pyridine. To confirm that this pretreatment did not affect the structure of the RLDHs, the XRD patterns were recorded after a sample was treated under the same conditions. In each case the XRD patterns were unchanged. In the IR spectra (Figure 9) of U-RLDH(3) and T-RLDH, bands recorded at about 1600, 1490, and 1450 cm^{-1}, can be attributed to the 8a, 19a, and 19b modes of pyridine molecules coordinated to surface Lewis acid sites. The splitting observed for the 8a band (1612, 1602, and 1596 cm^{-1}) has been ascribed to the presence of different types of Lewis acid sites; the band at 1596 cm^{-1} has also been ascribed to hydrogen-bonded pyridine molecules.[38,39] These results indicate that both basic and acidic hydroxyl groups are present in the RLDHs.

Catalytic activity

The catalytic activity of U-RLDHs and T-RLDH were tested in the self-condensation of acetone using different catalyst loadings and at different temperatures. Figure 10 shows a comparison of the catalytic performance of U-RLDH(3) and T-RLDH. It can be seen in Figure 10A, for U-RLDH(3) with acetone/catalyst = 2 mol/0.3 g, the conversion of acetone to DAA increases with reaction time and after 560 min reaches 22.8% at 273 K, which is very close to the thermodynamic equilibrium conversion (23.1%).[40] No detectable amounts of other possible condensation products were present. However, under the same reaction conditions, the conversion of acetone to DAA with T-RLDH reaches 20.4% after 1440 min at 273 K, which is close to that reported in the literature for catalysts synthesized by titration co-precipitation.[17,20] With a higher loading of catalyst (acetone/catalyst = 0.075 mol/0.3 g) at the same temperature, the conversion of acetone with U-RLDH(3) reaches the thermodynamic equilibrium after only 44 min, whilst 210 min is required to reach equilibrium with T-RLDH as the catalyst (Figure 10B). At 293 K with acetone/catalyst = 2 mol/0.3 g (Figure 10C), the conversion of acetone with U-RLDH(3) reaches the thermodynamic equilibrium conversion (12.1%)[40] after 180 min whilst with T-RLDH equilibrium is attained after 320 min. The above results show that activated MgAl-LDH synthesized by urea decomposition, U-RLDH(3), has higher catalytic activity than the catalyst prepared by titration co-precip-

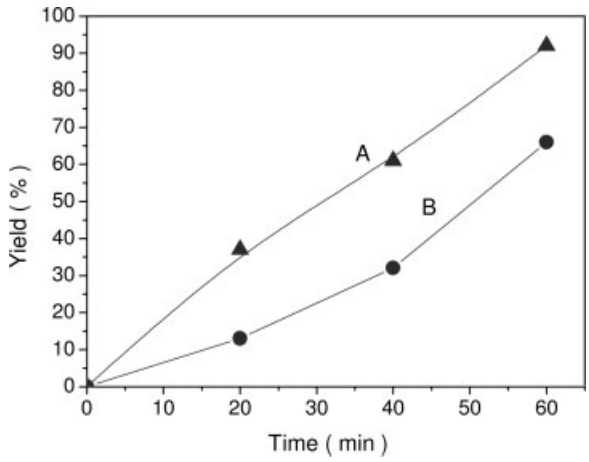

Figure 11. The yield of benzylidenemalononitrile in the Knoevenagel reaction with different catalysts: (A) U-RLDH (3); (B) T-RLDH.

Table 2. Physicochemical Properties and Catalytic Data of Activated LDH Samples

Catalyst	T-RLDH	U-RLDH(3)	U-RLDH(10)
Mg/Al molar ratio	2.05	1.97	1.92
%C	0.867	1.224	–
Lattice parameter *a*/nm	0.301	0.303	0.305
Lattice parameter *c*/nm	2.294	2.247	2.313
Crystallite size in *a* direction/nm (A)*	180	3900	4200
Crystallite size in *c* direction/nm (C)†	66.4	84.9	85.4
Aspect ratio A/C	2.71	45.9	49.2
Most probable particle size‡/nm	250	3460	3970
Specific surface area/m^2/g	185	141	143
Surface area of planes perpendicular to *ab*§/m^2/g	14.53	0.71	0.67
Surface area of planes parallel to *ab*§/m^2/g	170.47	140.29	142.33
Acetone conversion to DAA after 60 min/%¶	3.0	8.3	9.2
Acetone conversion to DAA after 180 min/%¶	10.2	15.8	16.6
Acetone conversion to DAA after 300 min/%¶	14.4	19.6	20.2
Time to reach equilibrium/min¶	1730	560	480

*Measured from SEM and TEM micrographs.
†Calculated from the values of the full width at half-maximum (FWHM) of the (003) diffraction peaks by means of the Scherrer formula: $C = 0.89\lambda/\beta\cos\theta$, where β is the FWHM of the X-ray line, θ is the Bragg diffraction angle of the peak, λ is the wavelength of X rays (0.15406 nm).
‡Measured by laser light scattering.
§Surface area of planes parallel to *ab* (S_A)/Surface area of planes perpendicular to *ab* (S_C) = $(3^{0.5}/4)A/C = 0.433A/C$; $S_A + S_C$ = Specific surface area.
¶The conversion of acetone to DAA over different catalysts at 273 K with acetone/catalyst = 2 mol/0.3 g.

itation, T-RLDH. It should be noted that during the process of drafting this manuscript, Greenwell et al. have also reported the same experimental result.[41] The activation of LDHs via calcination and rehydration is considered to involve the replacement of interlayer and surface carbonate by OH^- anions. In our experiments, it was found that U-LDHs, T-LDH, U-LDOs, and T-LDO have no significant catalytic activity in the self-condensation of acetone, the main reason being that there are few OH^- anions on the surface of these samples.

For the Knoevenagel reaction of malononitrile with benzaldehyde to afford benzylidenemalonoritrile, the same trend was found as for the self-condensation of acetone. As shown in Figure 11, the catalytic activity of U-RLDH(3) is significantly higher than that of T-RLDH.

Acid-base bifunctional catalysis mechanism

The physicochemical properties and catalytic data for U-RLDH(3), U-RLDH(10), and T-RLDH are shown in Table 2. Elemental analysis indicates that the compositions of the three samples are very similar. LDHs are invariably contaminated by carbonate anions, even where preparation is carried out under nitrogen, but elemental analysis shows that the amount of carbonate incorporated in the sample is low, indicating that hydroxide ions comprise the majority of the interlayer anions. Furthermore, the Mg/Al ratios are close to 2 in each case; this implies that the layer charge density and hence loading of hydroxide anions are comparable in the three samples. Thus, the variation in catalytic performance of the materials is not a result of different anion content. Powder XRD (Figure 1), electron microscopy (Figure 2), laser particle size analysis (Figure 5), and BET surface area measurements (Table 2) are consistent in indicating that the crystallinity of the U-RLDHs is higher than that of T-RLDH. The catalytic activities of the three activated LDHs were tested in acetone condensation. In each case, overall conversions to DAA close to the thermodynamic equilibrium value were obtained. The rate of conversion of acetone to DAA decreases in the order of U-RLDH(10) > U-RLDH(3) $\gg$ T-RLDH (see Table 2).

These results are in marked contrast to most of those in the literature. It has been reported[22] that the activity of activated LDHs in aldol reactions shows a correlation with overall surface area (in the range 200–400 $m^2\ g^{-1}$). Other studies[17,21] have indicated that the catalytic activity increases with decreasing lateral size of the LDH particles (in the range 20–430 nm). Since reducing the lateral dimensions of the crystallites leads an increase in exposed edge area and number of edge sites, it has been suggested that only the basic sites on the edges of LDH-platelets at the entrance to the interlayer galleries (~5% of the total basic sites) are accessible to the substrate. In our case, the U-RLDH materials, which have a large lateral size (~4000 nm) and relatively low surface area (~140 $m^2\ g^{-1}$), have a much higher activity than T-RLDH, despite the much smaller lateral size and higher surface area of the latter (see Table 2). Assuming a hexagonal geometry, the proportion of the surface area contributed by the hexagonal (*ab*) surfaces and edge surfaces can be correlated[17] with the aspect ratio (see Table 2). The edge surface area of T-RLDH is much larger than that of the U-RLDHs, suggesting that the activities of our materials are not related to the areas of the exposed edge surfaces, and an alternative explanation is required.

Roeffaers et al. have adapted real time monitoring of the chemical transformation of individual organic molecules by fluorescence microscopy to monitor reactions catalysed by a crystal of an LDH with the formula $[LiAl_2(OH)_6]^+(OH)^-\cdot nH_2O$.[42] They found the activity of base catalysis by LDH is not always associated with the same type of hydroxyl groups and that transesterification occurs mainly at the {0001} plane. When OH^- anions were introduced in the interlayer via calcination/rehydration, the CO_3^{2-} and other anions on the surface were also replaced by OH^- anions. Furthermore,

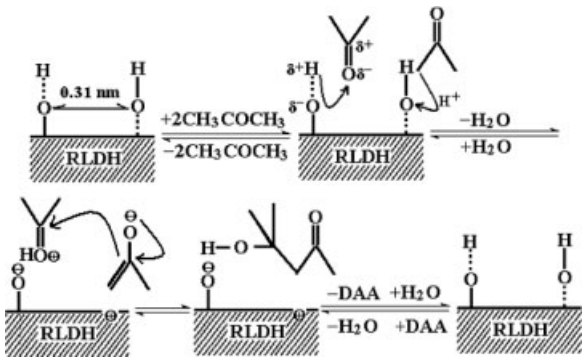

Scheme 1. Proposed acid-base bifunctional catalytic mechanism of the self-condensation of acetone on activated LDHs (RLDH).

other experiments demonstrate that the hydroxyl groups are arranged in an ordered manner on the LDH surface. For example, it has been shown that the LDH surface can act as a macroligand providing an ordered array of OH and O^- groups which facilitates the assembly of trimeric $Ru^{IV}Mn^{IV}Mn^{IV}$ units *in situ* on the surface.[43] The resulting material is an active catalyst for the liquid-phase oxidation of alcohols. Our results from adsorption experiments with phenol and pyridine as well as HRTEM (see Figure 3) indicate that there are both acidic and basic hydroxyl groups on the surface of LDHs that can form acid-base pairs with a separation of 0.31 nm. Very recently, Kaneda and coworkers[24] have also suggested that RLDHs possesses a highly effective acid-base bifunctional surface capable of mediating the Knoevenagel and Michael reactions. Therefore, we propose the following acid-base mechanism for the aldol reaction on activated RLDHs to interpret their catalytic behavior. As shown in Scheme 1, a weak acid site can interact with the carbonyl group of acetone polarizing the C=O bond and increasing the density of positive charge on the carbon of the carbonyl group. This makes the carbon more susceptible to attack by the enolate anion of acetone formed by interaction with an adjacent basic site on the surface of the LDH. One C—C bond, a C—O bond, and an O—H bond in DAA are formed between an acid-base pair. The lengths of these bonds are about 0.15, 0.14, and 0.10 nm, respectively. Taking into account the bond angles, the effective length of the three bonds is closely matched with the distance between two OH groups. There are only relatively few active acid-base hydroxyl pairs with an OH—OH distance of 0.31 nm on the surface of T-RLDH because of its poor crystallinity. In contrast, the high crystallinity and large particle size of U-RLDHs results in a regular arrangement of hydroxyl groups on the surface and a high density of appropriately separated acid-base pairs. The proposed acid-base catalytic mechanism explains the higher activity of the U-RLDHs compared with T-RLDH. This mechanism also accounts for the high selectivity of acetone condensation on activated LDH catalysts. A similar mechanism can be envisaged for the Knoevenagel reaction of malononitrile with benzaldehyde to afford benzylidenemalonoritrile, to account for the higher activity of U-RLDH as a catalyst for this reaction.

Conclusions

Activated MgAl-LDHs synthesized by urea hydrolysis have a much higher activity in aldol and Knoevenagel reactions than the corresponding material synthesized by the coprecipitation method. We suggest that catalysis of the reactions by LDHs requires the presence of acid-base hydroxyl pairs and that catalytic activity is maximized for highly crystalline structures with an ordered array of surface hydroxyl groups. The proposed acid-base catalytic mechanism explains the higher activity of the activated LDHs with high crystallinity. This demonstration of the ability of regular lattice positions, rather than defect sites, to act as catalytic active sites, should stimulate the development of new types of catalysts.

Acknowledgments

The National Natural Science Foundation of China (Project No: 20541003), the National Natural Science Foundation Major International Joint Research Program of China (Project No. 20620130108) and the 111 Project of China are acknowledged for financial support.

Literature Cited

1. Ertl G, Knoezinger H, Weitkamp J. *Handbook of Heterogeneous Catalysis*. Weinheim: VCH, 1997.
2. Johanek V, Alurin M, Grant AW, Kasemo B, Henry CR, Kasemo B, Henry CR, Libuda J. Fluctuations and bistabilities on catalyst nanoparticles. *Science*. 2004;304:1639–1650.
3. Thomas JM, Terasaki O. The electron microscope is an indispensable instrument for the characterization of catalysts. *Top Catal*. 2002; 21:155–159.
4. Weckhuysen BM. Determining the active site in a catalytic process: operando spectroscopy is more than a buzzword. *Phys Chem Chem Phys*. 2003;5:4351–4360.
5. Wells DH, Delgass WN, Thomson KT. Evidence of defect-promoted reactivity for epoxidation of propylene in titanosilicate (TS-1) catalysts: a DFT study. *J Am Chem Soc*. 2004;126:2956–2962.
6. Campbell CT. The active site in nanoparticle gold catalysis. *Science*. 2004;306:234–235.
7. Thomas JM, Thomas WJ. *Principles and Practice of Heterogeneous Catalysis*. Weinheim: VCH, 1996.
8. Lince JR, Carre DJ, Fleischauer PD. Effects of argon ion bombardment on the basal plane surface of MoS_2. *Langmuir*. 1986;2:805–808.
9. Iglesia E, Barton DG, Biscardi JA, Gines MJL, Soled SL. Bifunctional pathways in catalysis by solid acids and bases. *Catal Today*. 1997;38:339–360.
10. Climent MJ, Corma A, Fornés V, Guil-Lopez R, Iborra S. Aldol condensations on solid catalysts: a cooperative effect between weak acid and base sites. *Adv Synth Catal*. 2002;344:1090–1096.
11. Rives V. *Layered Double Hydroxides: Present and Future*. New York: Nova Science Publishers, 2001.
12. Climent MJ, Corma A, Iborra S, Velty A. Activated hydrotalcites as catalysts for the synthesis of chalcones of pharmaceutical interest. *J Catal*. 2004;221:474–482.
13. Kantam ML, Choudary BM, Reddy CV, Rao KK, Figueras F. Aldol and Knoevenagel condensations catalysed by modified Mg-Al hydrotalcite: a solid base as catalyst useful in synthetic organic chemistry. *Chem Commun*. 1998;1033–1034.
14. Sychev M, Prihod'ko R, Erdmann K, Mangel A, Van Santen RA. Hydrotalcites: relation between structural features, basicity and activity in the Wittig reaction. *Appl Clay Sci*. 2001;18:103–110.
15. Choudary BM, Kantam ML, Reddy CV, Rao KK, Figueras F. Henry reactions catalysed by modified Mg-Al hydrotalcite. *Green Chem*. 1;146:187–189.
16. Abéllo S, Medina F, Tichit D, Ramirez JP, Groen JC, Sueiras JE, Salagre P, Cesteros Y. Aldol condensations over reconstructed Mg-Al hydrotalcites: structure-activity relationships related to the rehydration method. *Chem Eur J*. 2005;11:728–739.

17. Roelofs JCAA, Lensveld DJ, Van Dillen AJ, De Jong KP. On the structure of activated hydrotalcites as solid base catalysts for liquid-phase aldol condensation. *J Catal*. 2001;203:184–191.
18. Tichit D, Bennani MN, Figueras F, Tessier R, Kervennal J. Aldol condensation of acetone over layered double hydroxides of the meixnerite type. *Appl Clay Sci*. 1998;13:401–415.
19. Prinetto F, Tichit D, Teissier R, Coq B. Mg- and Ni-containing layered double hydroxides as soda substitutes in the aldol condensation of acetone. *Catal Today*. 2000;55:103–116.
20. Roelofs JCAA, Van Dillen AJ, De Jong KP. Base-catalyzed condensation of citral and acetone at low temperature using modified hydrotalcite catalysts. *Catal Today*. 2000;60:297–303.
21. Winter F, Van Dillen AJ, De Jong KP. Supported hydrotalcites as highly active solid base catalysts. *Chem Commun*. 2005;3977–3979.
22. Abelló S, Medina F, Tichit D, Pérez-Ramírez J, Cesteros Y, Salagre P, Sueiras JE. Nanoplatelet-based reconstructed hydrotalcites: towards more efficient solid base catalyst in aldol condensations. *Chem Commun*. 2005;1453–1455.
23. Zhang H, Qi R, Evans DG, Duan X. Synthesis and characterization of a novel nano-scale magnetic solid base catalyst involving a layered double hydroxide supported on a ferrite core. *J Solid State Chem*. 2004;177:772–780.
24. Ebitani K, Motokura K, Mori K, Mizugaki T, Kaneda K. Reconstructed hydrotalcite as a highly active heterogeneous base catalyst for carbon-carbon bond formations in the presence of water. *J Org Chem*. 2006;71:5440–5447.
25. Oh JM, Hwang SH, Choy JH. The effect of synthetic conditions on tailoring the size of hydrotalcite particles. *Solid State Ionics*. 2002;151:285–291.
26. Ogawa M, Kaiho H. Homogeneous precipitation of uniform hydrotalcite particles. *Langmuir*. 2002;18:4240–4242.
27. Pagano MA, Forano C, Besse JP. Synthesis of Al-rich hydrotalcite-like compounds by using the urea hydrolysis reaction-control of size and morphology. *J Mater Chem*. 2003;13:1988–1993.
28. Costantino U, Marmottini F, Nocchetti M, Vivani R. New synthetic routes to hydrotalcite-like compounds—characterisation and properties of the obtained materials. *Eur J Inorg Chem*. 1998;10:1439–1446.
29. Yao K, Taniguchi M, Nakata M, Yamagishi A. Electrochemical STM observation of $[Fe(CN)_6]^{3-}$ ions adsorbed on a hydrotalcite crystal surface. *J Electroanal Chem*. 1998;458:249–252.
30. Yao K, Taniguchi M, Nakata M, Takahashi M, Yamagishi A. Electrochemical scanning tunneling microscopy observation of ordered surface layers on an anionic clay-modified electrode. *Langmuir*. 1998;14:2890–2896.
31. Sing KSW, Everett DH, Haul RAW, Moscou L, Pierotti RA, Rouquerol J, Siemieniewska T. Reporting physisorption data for gas/solid systems with special reference to the determination of surface area and porosity. *Pure Appl Chem*. 1985;57:603–619.
32. Parida K, Das J. Mg/Al hydrotalcites: preparation, characterisation and ketonisation of acetic acid. *J Mol Catal A*. 2000;151:185–192.
33. Lima E, Laspéras M, De Ménorval LC, Tichit D, Fajula F. Characterization of basic catalysts by the use of nitromethane as NMR probe molecule and reactant. *J Catal*. 2004;223:28–35.
34. Prinetto F, Ghiotti G, Durand R, Tichit D. Investigation of acid-base of catalysts obtained from layered double hydroxides. *J Phys Chem B*. 2000;104:11117–11126.
35. Di Cosimo JI, Diez VK, Apesteguia CR. Synthesis of α, β-unsaturated ketones over thermally activated Mg-Al hydrotalcites. *Appl Clay Sci*. 1998;13:433–449.
36. Li F, Jiang XR, Evans DG, Duan X. Structure and basicity of mesoporous materials from Mg/Al/In layered double hydroxides prepared by separate nucleation and aging steps method. *J Porous Mater*. 2005;12:55–63.
37. Rousselot I, Taviot-Gueho C, Besse JP. Synthesis and characterization of mixed Ga/Al-containing layered double hydroxides: study of their basic properties through the Knoevenagel condensation of benzaldehyde and ethyl cyanoacetate, and comparison to other LDHs. *Int J Inorg Mater*. 1999;1:165–174.
38. Chisem IC, Jones W, Martin I, Martin C, Rives V. Probing the surface acidity of lithium aluminium and magnesium aluminium layered double hydroxides. *J Mater Chem*. 1998;8:1917–1925.
39. Del Arco M, Gutierrez S, Martin C, Rives V. FTIR study of isopropanol reactivity on calcined layered double hydroxides. *Phys Chem Chem Phys*. 2001;3:119–126.
40. Podrebarac GG, Ng FTT, Rempel GL. A kinetic study of the aldol condensation of acetone using an anion exchange resin catalyst. *Chem Eng Sci*. 1997;52:2991–3002.
41. Greenwell HC, Holliman PJ, Jones W, Velasco BV. Studies of the effects of synthetic procedure on base catalysis using hydroxide-intercalated layered double hydroxides. *Catal Today*. 2006;114:397–402.
42. Roeffaers MBJ, Sels BF, Uji-I H, De Schryver FC, Jacobs PA, De Vos DE, Hofkens J. Spatially resolved observation of crystal-face dependent catalysis by single turnover counting. *Nature*. 2006;439:572–575.
43. Ebitani K, Motokura K, Mizugaki T, Kaneda K. Heterotrimetallic RuMnMn species on a hydrotalcite surface as highly efficient heterogeneous for liquid-phase oxidation of alcohols with molecular oxygen. *Angew Chem Int Ed*. 2005;44:3423–3426.

Manuscript received May 11, 2006, and revision received Dec. 18, 2006.